Hybrid Solid-State Qubits: The Powerful Role of Electron Spins

John J.L. Morton[1,2] and Brendon W. Lovett[1,3]

[1]Department of Materials, University of Oxford, Oxford OX1 3PH, United Kingdom; emails: john.morton@materials.ox.ac.uk, brendon.lovett@materials.ox.ac.uk

[2]Clarendon Laboratory, University of Oxford, Oxford OX1 3PU, United Kingdom

[3]Current address: School of Engineering and Physical Sciences, Heriot-Watt University, Edinburgh, EH14 4AS, United Kingdom

Annu. Rev. Condens. Matter Phys. 2011. 2:189–212

First published online as a Review in Advance on December 3, 2010

The *Annual Review of Condensed Matter Physics* is online at conmatphys.annualreviews.org

This article's doi: 10.1146/annurev-conmatphys-062910-140514

1947-5454/11/0310-0189$20.00

Keywords

quantum information, electron spin, magnetic resonance, decoherence, hybrid qubits

Abstract

We review progress on the use of electron spins to store and process quantum information, with particular focus on the ability of the electron spin to interact with multiple quantum degrees of freedom. We examine the benefits of hybrid quantum bits (qubits) in the solid state that are based on coupling electron spins to nuclear spins, electron charge, optical photons, and superconducting qubits. These benefits include the coherent storage of qubits for times exceeding seconds; fast qubit manipulation; single qubit measurement; and scalable methods for entangling spatially separated, matter-based qubits. In this way, the key strengths of different physical qubit implementations are brought together, laying the foundation for practical solid-state quantum technologies.

Quantum bit (qubit): two-level quantum system that is the basic building block of a quantum computer

1. INTRODUCTION

If the full potential of quantum information processing can be realized, its implications will be far reaching across a range of disciplines and technologies. The extent of these implications is certainly not yet fully known, but the revolutionary effect that quantum physics would have on cryptography, communication, simulation, and metrology is well established (1, 2).

Even though building a quantum computer is very challenging, research focused on achieving this goal can already claim to have produced some of the most high-impact scientific results of the past decade. One reason is that the language of quantum information has shown how to bring together and find new links between work on a staggering variety of physical systems.

The past 15 years have seen candidate embodiments of quantum bits (qubits) tested to their limits of coherence time, and in some cases control over a small number of such systems has become refined enough to permit the demonstration of basic quantum logic gates. However, there has been an increasing awareness that the challenge of faithfully storing, processing, and measuring quantum information within physical systems is sufficiently great so as to discourage relying on one quantum degree of freedom alone. Furthermore, classical information processors use different physical systems to encode information at different stages of their operation: for example, charge states, in semiconductors for processing information; the orientation of magnetic domains, in hard disks for longer-term storage; and optical photons, for transmitting data.

For a quantum computer to benefit from such an optimized use of resources, it must be able to transfer quantum information coherently between different degrees of freedom. Within the solid state, the electron spin exhibits a number of interactions that could be harnessed for this hybridizing of quantum information: with nuclear spins that benefit from long coherence times, or with charge or optical states, either of which could be used to measure, manipulate, or even entangle electron spins (see **Figure 1**).

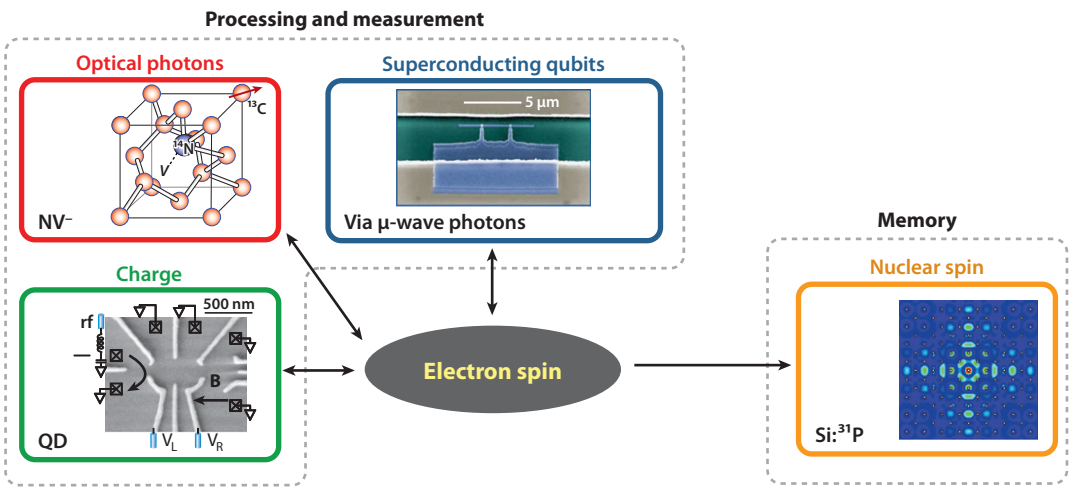

Figure 1

Electron spins in the solid state interact with several other degrees of freedom, including nuclear spins, optical photons, charge and, potentially, superconducting qubits via circuit quantum electrodynamics. In each case, example systems are illustrated. Such interactions can be harnessed to enhance the processing, coherent storage, and measurement of quantum information. [Figure includes extracts from References 2 and 3 with permission from Macmillan Publishers Ltd; 142, Copyright (2009) by the American Physical Society **http://prl.aps.org/abstract/PRL/v103/i16/e160503**; and 162 with permission from Anais da Academia Brasileira de Ciências.]

In this review we examine the ways in which electron spin qubits may couple to different degrees of freedom in the solid state and how this is being used to hybridize quantum information. We distinguish between two regimes of coupling:

1. A weak interaction that provides an opportunity to transfer some (small) amount of classical information between the electron spin and another degree of freedom. This kind of interaction can be very important in few-to-single spin measurement, for example, a small change in conductivity or photoluminescence depending on the state of an electron spin.
2. A stronger interaction capable of providing the coherent transfer of a quantum state between two degrees of freedom, with sufficient fidelity to permit the storage of quantum information or performing entangling operations.

Quantum dot (QD): semiconductor structure in which electrons can be confined, in all three dimensions, on a nanometer length scale

2DEG: two-dimensional electron gas

Hole: quasiparticle generated when an electron is removed from the valence band; heavy holes are those close to the band edge with large effective mass

2. ELECTRON SPIN QUANTUM BITS

To understand how to use electron spins linked with other degrees of freedom in hybrid quantum processor architectures, we must first understand the different forms that electron spin qubits can take. In this section, we examine some important implementations of electron spin qubits, with a particular focus on those in the solid state.

2.1. Quantum Dots: Artificial Atoms

Quantum dots (QDs) are artificial structures that are fabricated so that electronic states are confined, on a nanometer length scale, in all three spatial dimensions. They are typically divided into two broad classes. First, there are lithographically defined structures consisting of a quantum-well semiconductor heterostructure that confines a two-dimensional electron gas (2DEG). The other dimensions are defined by lithographically deposited electrical top gates, (for an example configuration, see **Figure 1**). This allows one, two, or more dots to be deposited side by side; gate electrodes are used to control the number of charges within the structure, and allow a single-electron spin to be isolated.

The second class of QDs are self-assembled nanostructures in which confinement is naturally provided in all three dimensions. They are typically fabricated by molecular beam epitaxy: A large band-gap semiconductor forms the substrate, and a smaller band-gap material is deposited on top (see **Figure 2*a***). Under the right conditions, nanoscale islands form, and subsequent overgrowth of the original material leads to three-dimensional confinement. The resultant discrete energy-level structure of both conduction and valence bands is shown in **Figure 2*b*** and allows the physics of small numbers of electrons and holes to be investigated. The spin properties of both types of carrier are essentially determined by the corresponding bulk properties. In group IV or III-V semiconductors, valence states have *p*-like orbitals, and can have total spin $J = 3/2$ or 1/2, whereas conduction states have *s*-orbital symmetry and have spin $J = 1/2$ (4). The confinement splits the six possible hole bands into three discrete doublets. The heavy holes ($J = 3/2$, $J_z = 3/2$ for growth direction z) generally have the largest effective mass of the valence states and under confinement form the highest lying doublet.

Analogous to bulk semiconductors, optical QDs can be either intrinsic (i.e., have full valence and empty conduction states), or doped to generate single-electron or single-hole ground states. Both are promising qubits and have been investigated experimentally (5–7) and theoretically (8, 9), though most work has focused on the electron spin (10, 11). Interband (or, more correctly, interstate) transitions typically lie in the optical or near-infrared region and can have significant transition dipole matrix elements (2, 12). These optically active transitions are the essential ingredient for an electron-photon interface, as discussed in Section 4.

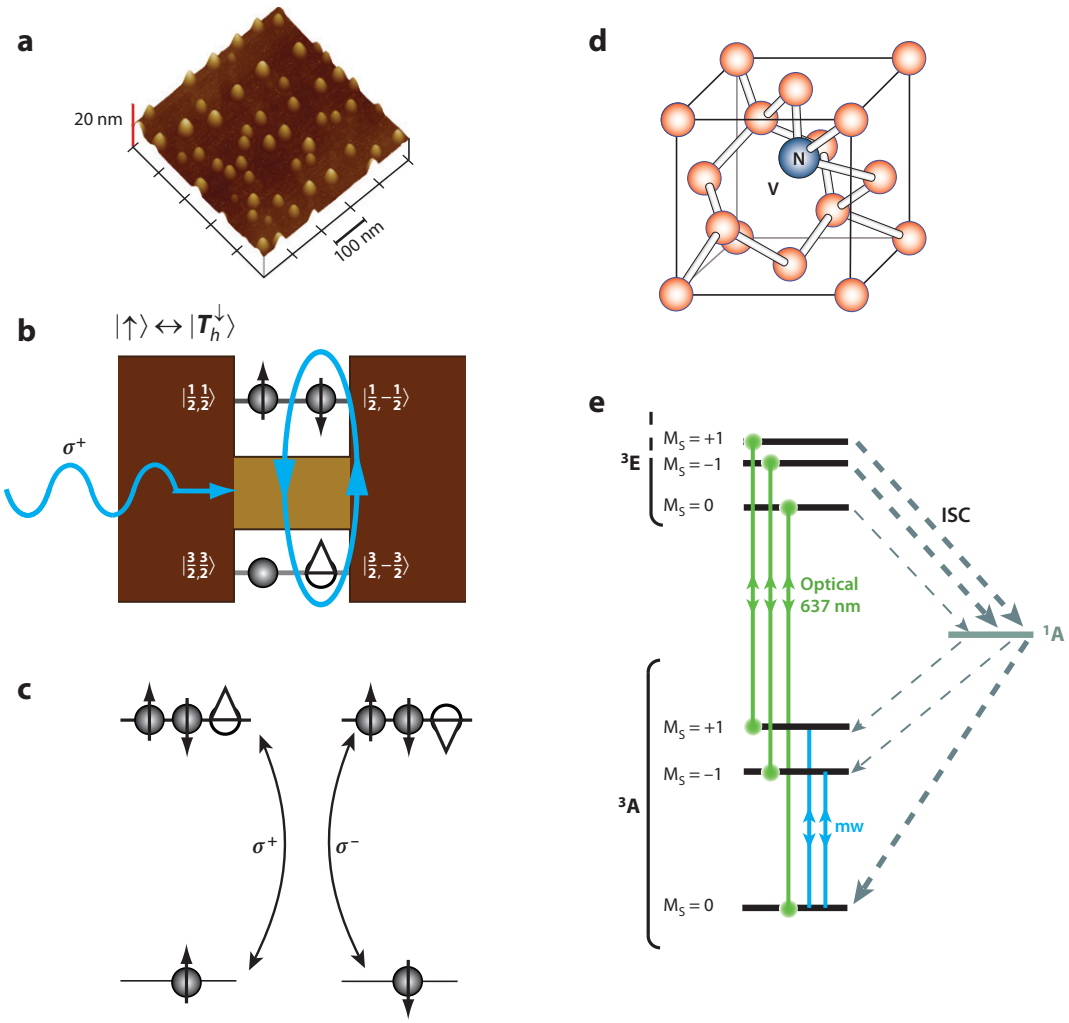

Figure 2

(*a*) Atomic force microscopy (AFM) micrograph showing the spontaneous formation of quantum dots (QDs) when a smaller band-gap material (*light brown*) is deposited on a larger band-gap substrate (*dark brown*). (*b*) Confinement potential in a cut through one such QD, showing discrete bound states with angular momentum $|J, J_z\rangle$. Here the QD is doped with a single electron, and excitation with σ^+ light leads to trion formation only for an initial $|\uparrow\rangle$ spin state. (*c*) Spin selection rules for both kinds of polarized light. (*d*) Crystal structure and (*e*) electronic energy-level diagram of the NV^- center. Abbreviation: ISC, intersystem crossing. (Figure partly adapted and reprinted with permission from Reference 2.)

2.2. Impurities in Solids

The confinement achieved in QDs is naturally found in certain impurity or defect states within various materials, some of which provide ideal hosts for an associated electron spin. Desirable properties of the host material include a low natural abundance of nuclear spins (such as C, Si, Ge and certain II-VI-based materials) and weak spin-orbit coupling.

In the semiconductor industry, silicon is doped with phosphorous to increase the bulk electron concentration; however, at low temperatures the electron associated with the donor becomes bound to the P impurity. In his influential proposal (13), Kane suggested using arrays

of P-donors in silicon (Si:P) as nuclear spin qubits, whose interactions could be tuned by electrical top gates that change the wavefunction is the bound electron. This, and related proposals for Si:P quantum computing (14, 15), is well supported by a number of findings and achievements made over the past decade: among others *a*) control of P-donor placement in silicon with atomic precision using scanning probe methods (16); *b*) manipulation of donor wavefunctions through electrical gates (17–19); *c*) single-spin detection in silicon (20); and *d*) measurement of very long electron and nuclear coherence times, both in the range of 3–10 s, within a ^{28}Si isotopically enriched environment (21; A.M. Tyryshkin & S.A. Lyon, unpublished observation).

Other donors in silicon possess properties that make them of interest as electron spin qubits (22). For example, bismuth has a large nuclear spin ($I = 9/2$), offering a large Hilbert space for storing quantum information (23, 24), and its large hyperfine coupling ($A = 1.475$ GHz) gives a zero-field splitting that may be useful for coupling to superconducting resonators (25, 26).

The paramagnetic nitrogen-vacancy NV^- center in diamond has an $S = 1$ ground state, with a zero-field splitting between the $m_s = 0$ and $m_s = \pm 1$ states of ~2.88 GHz (see **Figure 2*d*,*e***). It exhibits coupling to surrounding ^{13}C nuclei and the local nitrogen nuclear spin (27), and possesses a highly advantageous optical transition that enables initialization and single-spin measurement (28), as discussed in detail in Section 4. In addition, NV^- centers offer the benefit of long coherence times at room temperature—1.8 ms in ^{12}C-enriched diamond (29)—which permits the measurement of coupling between NV^- centers separated by distances as long as 100 Å (30) (see also sidebar on Single-Spin Electron Spin Resonance).

SINGLE-SPIN ELECTRON SPIN RESONANCE

Some of the approaches described here could be extended to enable general single-spin electron spin resonance (ESR).

1. Cavities

The greatly reduced mode volume and high Q-factor of nanoscale superconducting resonators should lead to sufficient coupling between a single spin and the microwave field to permit single-spin ESR. Typical values of $Q \sim 10^5$, a cavity of volume 1 pL (1 μm^3), and frequency 1 GHz suggest a single spin will emit a scattered microwave photon every 10 ms (25).

2. Optics

Single NV^- electron spins can be measured close to the diamond surface and are sensitive to long-range dipolar coupling (30), enabling the indirect detection of other electron spins (154, 155). A nanocrystal of diamond could be mounted on a probe tip that scans over a surface, or the spins of interest could be deposited on a suitable diamond substrate.

3. Charge

Transport measurements of a carbon nanotube-based double QD device have shown the signature of coupling between a QD and a nearby electron spin (156). Carbon nanotubes can be controllably activated and functionalized with other molecular species (157). Combining such structures with magnetic resonance techniques could permit single-spin detection of an attached electron spin (158, 159).

ESR: electron spin resonance

ENDOR: electron-nuclear double resonance

NMR: nuclear magnetic resonance

There are other impurity spins with an associated optical transition that are at earlier stages of investigation, such as fluorine donors in II-VI semiconductors (31), whereas rare-earth impurities in glasses are being investigated as optical memories for quantum repeaters (32).

2.3. Molecular Electron Spin

Molecules offer highly reproducible components that can host electron spin and can be coupled together using the techniques of organic and inorganic chemistry. Simple organic radicals, such as those based on nitroxide radicals, are used extensively in the field of spin labeling for distance measurements in biological molecules (33). Their electron spin coherence times are limited to 1–10 μs in typical environments that are rich in nuclear spins from hydrogen nuclei, and can be extended to $\sim$100 μs for dilute spins in deuterated environments at 40 K (34).

Fullerenes, such as C_{60} and C_{82}, act as a molecular-scale trap for atoms or ions, shielding the electron spin of the caged species from the environment. Such endohedral fullerenes based on group III ions such as Sc-, Y-, and La@C_{82} possess T_2 times in excess of 200 μs under optimized conditions (35). (The notation $M@C_{xx}$ is used to indicate the species M is held within the C_{xx} fullerene cage.) In the case of the remarkable N@C_{60} molecule, atomic nitrogen occupies a high-symmetry position at the center of the cage, leading to an $S = 3/2$ electron spin with the longest coherence times of any molecular electron spin: 80 μs at room temperature rising to 500 μs at temperatures below 100 K (36, 37).

The organic radical created by X-ray irradiation of malonic acid crystals has been a standard in electron spin resonance (ESR) and electron-nuclear double resonance (ENDOR) spectrosocopy for many decades (38), and has also been used to explore methods of controlling coupled electron and nuclear spin qubits with a strong anisotropic hyperfine interaction (39, 40). Offering a large set of nondegenerate transitions, the high-spin ground state of many single-molecule magnets is capable in principle of hosting quantum algorithms such as Grover's search (41). Electron spin coherence (T_2) times up to a few microseconds have been measured (42), permitting Rabi oscillations in the electron spin to be observed (43). Despite their relatively short coherence times, these tunable systems may provide useful testbeds to explore quantum control of multilevel electron spin systems.

2.4. Spins of Free Electrons

Finally, it is possible to use free electrons as spin qubits. For example, using a piezoelectric transducer over a semiconductor heterostructure, surface acoustic waves can be launched into a 2DEG, such that each wave minimum contains a single electron (44). For more extreme isolation, electrons can be made to float above the surface of liquid helium, bound by their image charge. Electrical gates beneath the helium are used to direct the electrons around the surface with very high efficiency (45), enabling controlled interactions and measurement; meanwhile, their spin is expected to couple very weakly to the varying electrical potentials (46).

3. ELECTRON SPIN—NUCLEAR SPIN COUPLING

3.1. Electron Spins as a Resource for Nuclear Spin Qubits

Since the beginning of experimental studies into quantum information processing, nuclear spins and nuclear magnetic resonance (NMR) have provided a testbed for quantum control and logic

(47, 48). NMR can still claim to have hosted the most complex quantum algorithm to date, through the seven-qubit implementation of Shor's factoring algorithm (49). However, the weak thermal nuclear spin polarization at experimentally accessible temperatures and magnetic fields has limited the scalability of this approach, which relies on manipulating the density matrix to create states that are pseudo-pure (47, 48) and thus provably separable (50). A notable exception (albeit of limited scalability) is the use of a chemical reaction on parahydrogen to generate two nuclear spin states with a purity of ~0.92 (51).

Decoherence: loss of phase information in a quantum state or qubit, characterized by the decay time constant T_2

The magnetic moment of the electron spin is approximately 2,000 times greater, bringing several key benefits to nuclear spin qubits: *a*) enhanced spin polarization; *b*) faster gate manipulation time (10 ns for a typical electron spin single qubit rotation, rather than 10 μs for the nuclear spin); and *c*) more sensitive detection, via either bulk magnetic resonance or the more sensitive electrical or optical methods described in this review. The general spin Hamiltonian for an electron spin S coupled to one or more nuclear spins I_i in a magnetic field B is, in angular frequency units,

$$\mathcal{H} = \frac{g_e \mu_B}{\hbar} \vec{S} \cdot \vec{B} + \sum_i (\gamma_{n,i} \vec{I_i} \cdot \vec{B} + \vec{S} \mathbf{A}_i \vec{I_i}), \quad 1.$$

where g_e is the electron g-factor, μ_B the Bohr magneton, γ_n the nuclear gyromagnetic ratio, and $\mathbf{A}_i$ the hyperfine coupling tensor between the electron and nuclear spin. Additional terms, such as a zero-field splitting term $\vec{S}\mathbf{D}\vec{S}$, may appear in higher spin systems, such as NV^- centers in diamond.

For an electron and nuclear spin-half pair, this Hamiltonian leads to four levels, separately addressable through resonant pulses and typically in the microwave regime (10–100 GHz) for the electron spin (i.e., ESR) and in the radio-frequency regime (1–200 MHz) for the nuclear spin (i.e., ENDOR or NMR), as shown in **Figure 3*b***. By controlling the phase, power and duration of the pulse, qubit rotations around an axis perpendicular to the applied field are performed. Couplings that are stronger than the bandwidth of a typical pulse can be exploited to perform controlled-NOT (C-NOT), or similar operations, through a selective microwave or rf pulse. Weaker couplings can be used to perform conditional logic through a combination of pulses and delays, exploiting the difference in the time evolution of one spin depending on the state of the other.

Electron spin polarization can be indirectly (and incoherently) transferred to surrounding nuclear spins through a family of processes termed dynamic nuclear polarization, which is reviewed extensively elsewhere (52, 53). For strongly coupled nuclear spins, electron spin polarization can be transferred directly through the use of selective microwave and rf pulses—such a sequence forms the basis of the Davies ENDOR spectroscopic technique (54, 55). A complementary approach is to apply algorithmic cooling, which exploits an electron spin as a fast relaxing heat bath to pump entropy out of the nuclear spin system (56). The use of an optically excited electron spin (such as a triplet) can be advantageous, as *a*) it offers potentially large spin polarizations at elevated temperatures and *b*) the electron spin, a potential source of decoherence, is not permanently present (57).

Given an isotropic electron-nuclear spin coupling of sufficient strength, it is possible to perform phase gates (z-rotations) on nuclear spin qubits, on the timescale of an electron spin 2π microwave pulse, which is typically ~50 ns. The pulse must be selective on an electron spin transition in one particular nuclear spin manifold; hence, a weaker hyperfine coupling will necessitate a longer, more selective microwave pulse. This kind of geometric Aharanov-Anandan phase gate (58) was experimentally demonstrated using $N@C_{60}$ and Si:P-donor systems, and was used to dynamically decouple nuclear spins from strong driving fields

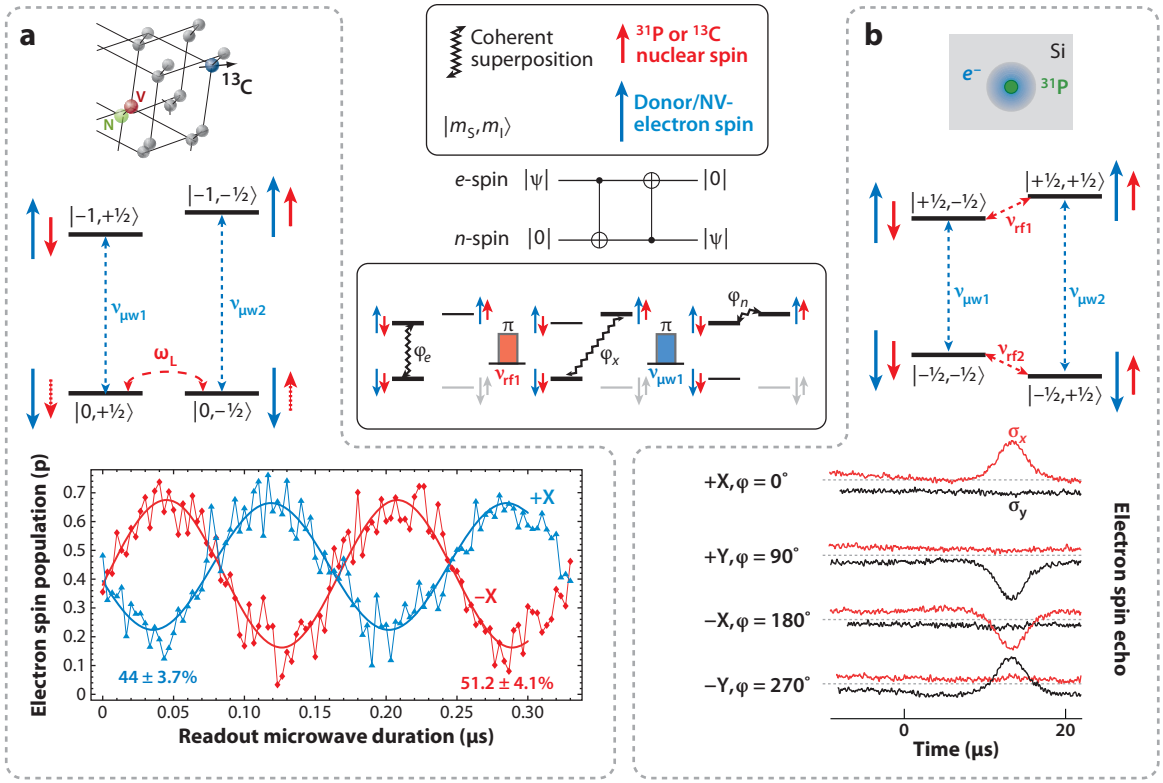

Figure 3

Two methods for coherently storing an electron spin state into a local, coupled nuclear spin. In both cases a SWAP operation is performed through two controlled-NOT (C-NOT) gates, which are achieved through a selective spin-flip. (*a*) Using the NV^- center in diamond, it is possible to achieve the nuclear spin-flip by exploiting the natural precession of the nuclear spin in the $m_S = 0$ electron spin manifold. A weak (∼20 G) magnetic field is applied perpendicular to the quantization axis, which is defined by the electron spin and orientation of the defect, causing an evolution ($\omega/2\pi$ ∼0.3 MHz) in the nuclear spin between $|\uparrow\rangle$ and $|\downarrow\rangle$. (*b*) The alternative, shown using P-donors in ^{28}Si, is to drive a nuclear spin-flip directly with a resonant radio-frequency pulse. In each case, electron spin coherence is generated; stored in the nuclear spin; and then retrieved some time later, which is considerably longer than the electron spin T_2. Observation of the recovered electron spin coherence can be achieved through Rabi oscillations, or by directly observing a spin echo, depending on the nature of the spin measurement used. (Panel *a* adapted from Reference 68, with permission from AAAS; panel *b* adapted from Reference 21, with permission from Macmillan Publishers Ltd.)

(59, 60). Given an anisotropic hyperfine coupling, the nuclear spin gate can be generalized to an arbitrary single-qubit rotation using a combination of microwave pulses and delays (40, 61). For multiple coupled nuclear spins and a correspondingly large Hilbert space, more elaborate control is needed (62), for example, using gradient ascent pulse engineering (63). These methods exploit an effect termed electron spin echo envelope modulation (ESEEM) in the ESR community (64, 65).

The weak and always-on coupling between two nuclear spins is another limitation of a nuclear spin-only NMR approach. Nuclear spin interactions can be decoupled through refocusing techniques—for example, using the ultrafast nuclear spin manipulations described above—however, methods for gating such interactions have also been explored. An example is the proposal of exploiting mutual coupling between two nuclear spins to

an intermediate electron spin that is optically excited (66). The mediator is diamagnetic in its ground state, such that the interaction between the two nuclei is effectively off. However, an optical pulse can excite a triplet state ($S = 1$) in the mediator, which can be manipulated using microwave pulses to produce gates of maximal entangling power between the two coupled nuclear spins. Preliminary ENDOR experiments on candidate functionalized fullerene molecules indicate that the key parameters of triplet polarization, relaxation rate and hyperfine coupling, are in the correct regime to permit this kind of gate (66).

Entanglement: exists in two or more qubits that cannot be described as a product of individual qubit states; leads to nonclassical correlations in qubit measurements

Given the above, it is clear that quantum logic between an electron and nuclear spin can also be performed. Entangling operations between them have been demonstrated in irradiated malonic acid crystals (39), and in the $N@C_{60}$ molecule (67); however, in both cases the spins were in a highly mixed initial state. Thus, only pseudo-entanglement was generated—the states were fully separable. Nevertheless, Reference 39 demonstrates an elegant way to perform density matrix tomography by separately varying the reference phase in the measurement of both the electron and nuclear spins. This type of procedure, if applied with high fidelity to spins at higher magnetic fields and lower temperatures, would lead to the demonstration of true electron-nuclear spin entanglement.

3.2. Nuclear Spin Quantum Memory

We may reverse the question, and ask how coupling to nuclear spins might offer advantages to electron spin qubits. One key advantage of the weak magnetic moment of nuclear spins is their correspondingly longer relaxation times T_1 (typically seconds to hours) and T_2 (typically seconds), which motivates the use of nuclear spins as quantum memories to coherently store the states of electron spin qubits. This has been achieved using *a*) NV^- centers and neighboring ^{13}C nuclei in diamond, exploiting the near-degeneracy of the nuclear spin levels in the $m_S = 0$ manifold (68); and *b*) ^{31}P-donor nuclear spins in isotopically purified ^{28}Si, where the nuclear spin is directly excited using a radio-frequency pulse (21). Both experiments are summarized in **Figure 3**.

The lifetime of the quantum memory is determined by the nuclear spin decoherence time T_{2n}, which was found to be $\gg 20$ ms in the case of ^{13}C in the NV^- diamond system at room temperature (68), and more than 2 s for the ^{31}P-donor nuclear spin. This approach has since been applied to other electron-nuclear spin systems such as the $N@C_{60}$ molecule ($T_{2n} = 140$ ms at 10 K) (R.M. Brown, A.M. Tyryshkin, K. Porfyrakis, E.M. Gauger, B.W. Lovett, et al., unpublished observation) and the substitutional nitrogen P1 center in diamond ($T_{2n} = 4$ ms at room temperature).

The large $I = 9/2$ nuclear spin of the ^{209}Bi-donor in silicon offers a large Hilbert space to store multiple electron spin coherences. Despite the wide range of nuclear transition frequencies (between 200 and 1,300 MHz at X-band), it is possible to implement the same coherence transfer sequence applied previously to P-donors (23). A further strength of this system is the ability to optically hyperpolarize the ^{209}Bi nuclear spin (24, 69), as was previously shown for the P-donor (70, 71).

An important limitation of the use of this kind of nuclear-spin quantum memory is that the nuclear spin coherence time is bounded by the electron spin relaxation time: $T_{2n} \leq 2T_{1e}$ (21). In many systems, T_{1e} can be made very long, for example, by operating at low temperatures; however, the ability to remove the electron spin, for example, through optical or electrical means, would simply eliminate this limit (15, 66).

Intersystem crossing (ISC): electronic transition between a singlet and a triplet, which is forbidden in lowest order

Trion: composite particle consisting of two electrons and one hole, or two holes and one electron

4. ELECTRON SPIN—OPTICAL PHOTON COUPLING

4.1. Mechanisms and Candidate Systems

There are various methods by which spin can couple to an optical transition in certain materials, exploiting some kind of spin-selective interaction with light. This interaction enables the initialization, manipulation, and measurement of single spins using optical techniques, which we review in this section.

NV^- centers (see **Figure 2*d,e***) possess an optically active level structure that has a number of fortuitous properties. In particular, there is an intersystem crossing (ISC) that can take place between the excited ^3E and a metastable singlet ^1A state, and the rate of ISC is three orders of magnitude faster for the $m_s = \pm 1$ excited states than for $m_s = 0$. Crucially, optical cycles between the ground and excited triplet states are essentially spin conserving, and relaxation from the ^1A state back to the triplet ground state ^3A occurs with greatest probability to the $m_s = 0$ state (72).

Spin selectivity in QDs is illustrated in **Figure 2*b,c***. A left (right) circularly polarized light pulse propagating in the z direction carries an angular momentum of $+\hbar(-\hbar)$ along the z axis, and if it is resonant with the heavy-hole to electron transition, will only excite the transition that has a net angular momentum loss (gain) of $\hbar$. Doping a QD with a single electron results in a spin-dependent optical transition for a given circular polarization. For example, if σ_+ light is incident on the sample propagating in the z direction, then a state consisting of two electrons and one hole (known as a trion) is only created from the $J_z = +1/2$ level. This kind of Pauli blocking forms the basis of methods for optical initialization, readout, and manipulation of spins in QDs.

Optical coupling to spin qubits has been explored in other systems, such as donors in silicon (71), but we focus here on NV^- and QD systems to illustrate the techniques and opportunities for coupling electron spins and photons in the solid state.

4.2. Electron Spin Initialization

Electron spins can become highly polarized in strong magnetic fields and low temperatures (e.g., 90% polarization at 2 K and 4 T). However, it is possible to use optical cooling to achieve similar polarizations at much lower magnetic fields and more accessible temperatures. The initialization of NV^- center spins at room temperature is possible because cycling the 637-nm optical transition largely preserves the electron spin state. As described above, the $m_s = 0$ state has a very low probability of undergoing ISC when in the excited state ^3E, whereas the $m_s = \pm 1$ states have some chance of crossing to ^1A, which will relax to $m_s = 0$. A few cycles are enough to generate a large spin polarization ($\sim$90%) in the $m_s = 0$ state (30, 73). Unfortunately, no method to increase this polarization closer to 100% has yet been identified; the difficulty is that the optical transitions are not perfectly spin-conserving, and so there is a finite chance of a spin-flip on each optical cycle (72).

Atatüre et al. (74) demonstrated laser-induced spin polarization in an InAs/GaAs QD (11). They use a σ^- laser to depopulate the $|\downarrow\rangle$ spin level, promoting population to the trion above (see **Figure 2*c***). The trion decays primarily back to the original state, but there is a small probability that it goes to the other low-lying spin level ($|\uparrow\rangle$) via a spin-flip Raman process that arises due to light-heavy hole mixing. However, any population in $|\uparrow\rangle$ will remain, because the pump has no effect on it. In this way, polarization builds up as eventually the $|\downarrow\rangle$ is completely emptied, so long as there is no direct spin-flip mechanism with a rate comparable with the forbidden decay rate. In zero magnetic field, interaction with the nuclear spin ensemble does lead to spin-flips, and only in an applied magnetic field can such flips be sufficiently suppressed.

The measurement of polarization is made by observing the change in transmission of the probe laser: Once the spin is polarized, no more absorption can occur. However, a sufficiently sensitive measurement can only be obtained by exploiting a differential transmission technique (75, 76).

Other methods of spin initialization rely on the generation of a polarized exciton in a diode-like structure that permits the preferential tunneling of either an electron or a hole out of the QD and into the bulk semiconductor contacts. Both electrons (77) and holes (6) can be prepared in this way.

4.3. Electron Spin Measurement

The spin-selective ISC in the excited ^{3}E state enables the measurement of the spin state of a single NV$^-$ center. The lifetime of the dark ^{1}A state ($\sim$250 ns) is more than an order of magnitude longer than that of ^{3}E, such that the fluorescence intensity of the center is reduced when ISC can occur (72). The act of measurement (cycling the ^{3}A-^{3}E optical transition to observe fluorescence) itself serves to reinitialize the spin in the $m_s = 0$ state, so the signature of the spin measurement is an $\sim$20% difference in fluorescence intensity in the first $\sim$0.5 μs of optical excitation. This means that each measurement must be repeated many times to build up good contrast between the different spin states. Experiments showing single-spin measurement are therefore a time-ensemble average—in contrast to the spin-ensemble average typical of ESR experiments—and refocusing techniques must be employed to remove any inhomogeneity (28).

Methods to improve the efficiency of the measurement are being actively explored, for example, using ^{13}C nuclear spins (78) or the ^{14}N nuclear spin (79) as ancillae for repeated measurement. The electron spin state is copied to ancilla(e) nuclear spin(s), and then measured. [This is not a cloning of the electron spin state (which is forbidden), but rather a C-NOT operation such that $\alpha|0_e 0_n\rangle + \beta|1_e 0_n\rangle \rightarrow \alpha|0_e 0_n\rangle + \beta|1_e 1_n\rangle$.] After some time ($<1$ μs), any useful information on the electron spin state ceases to be present in the fluorescence, and the electron spin is back in the $m_s = 0$ state; the ancilla state can be mapped back to the electron spin and the measurement repeated. Crucially, the coherent state of the coupled nuclear spin is not affected by the optical cycling that forms part of the electron spin measurement (68, 80).

A range of techniques for single-spin measurement have been explored for QDs. Several of these rely on the modification of refractive index that occurs close to (but not precisely at) optical resonance. By detuning a probe laser from resonance, absorption is suppressed and this dispersive regime can be exploited. Imagine, for example, a single-electron spin polarized in the $|\uparrow\rangle$ state. It will only interact with σ^+ light, and on passing through the QD region, light of this polarization will experience a slightly different optical path length to an unaffected σ^- beam. To enhance the difference in path lengths experienced, an optical microcavity can be exploited so that on average the light beam passes many times through the dot region. Linearly polarized light is composed of equal amounts of σ^+ and σ^-, and will therefore rotate on passing through the sample. The degree of rotation will be directly dependent on the magnitude and direction of the confined spin. The sensitivity of a typical measurement is improved by recording the degree of rotation as a function of detuning from resonance, and fitting the resulting curve with the initial spin polarization as a variable fitting parameter.

Berezovsky et al. (81) demonstrated this spin-dependent polarization rotation using a reflection geometry (which in this case is called the magneto-optical Kerr effect) to nondestructively read out a single spin following initialization in the $|\uparrow\rangle$ or $|\downarrow\rangle$ state. Atatüre et al. (82) performed similar measurements (see **Figure 4**), but using differential transmission to detect the rotation of polarization, which in this configuration is called Faraday rotation. State readout can also be

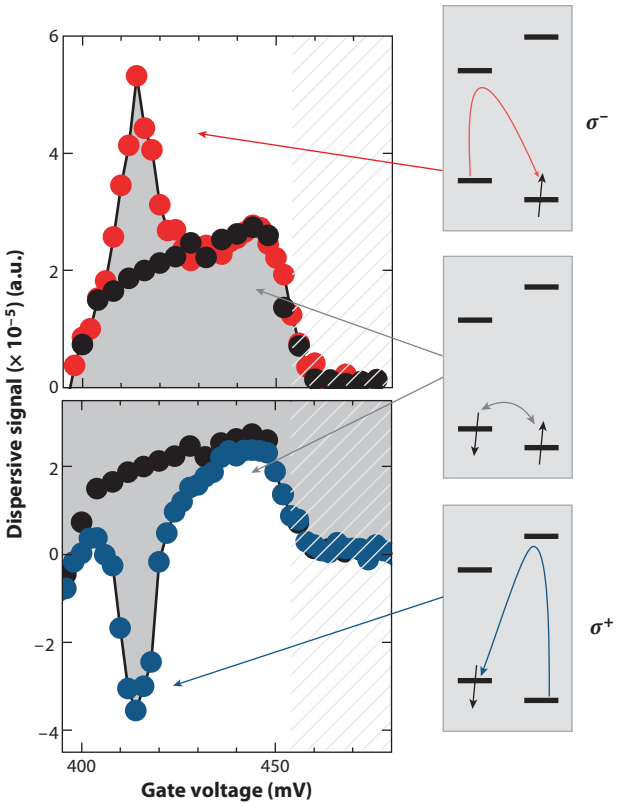

Figure 4

Experimental results of a preparation-measurement sequence for a spin in a quantum dot (QD). A preparation pulse is first applied with circular polarization, which results in spin pumping on resonance. Both panels show dispersive Faraday rotation (FR) measurements as a function of an applied gate voltage that is used to change the detuning of the preparation laser from resonance through the Stark shift it generates. The upper (*lower*) panel shows results using a σ^- (σ^+) preparation pulse. The black dots in each case represent the signal for a far-detuned preparation laser, with no spin cooling. The red (*blue*) dots show a preparation laser that is at resonance for a gate voltage of 415 mV, for the transitions shown on the right. A peak or dip in the FR signal is seen at resonance, which is a measurement of the prepared spin state. (Reprinted from Reference 82, with permission from Macmillan Publishers Ltd.)

achieved using a photocurrent technique, in which a trion that has been spin selectively created is allowed to tunnel from a QD in a diode structure (6, 77).

4.4. Electron Spin Manipulation

Once initialization and measurement are established, the stage is set for the observation of controlled single-spin dynamics. In the case of electron spins which are sufficiently long-lived, this can be performed by coupling the spin to a resonant microwave field, such as that used to observe coherent oscillations in a single NV^- electron spin between the $m_s = 0$ and the $m_s = \pm 1$ levels (28). Alternatively, by applying a magnetic field perpendicular to the direction of the initialization and measurement basis, it is possible to observe single-spin precession as a function of time between the initialization pump and Kerr rotation probe (10). For controlled

rotation around a second axis, an optical tipping pulse can be applied (83). This pulse is circularly polarized, and cycles around one of the spin selective transitions shown in **Figure 2*c***. If the pulse is resonant, and completes a cycle from spin to trion and back, a relative π phase shift is accumulated between the two spin states. [This is analogous to the nuclear spin phase gate described in Section 3.1, which is performed by driving the electron spin around a complete cycle. Similar phase gates can also be achieved in a photodiode system (6).] This corresponds to a rotation around the measurement basis axis, perpendicular to the applied field. Controlled rotation around two axes is sufficient for arbitrary single-qubit operations (1), though these experiments do not demonstrate how to stop the magnetic field precession. Greilich et al. (84) take the first step to overcoming this problem, first by demonstrating that an arbitrary angle phase gate can be achieved by detuning the cycling laser, and then by timing two $\pi/2$ phase gates such that a controlled field precession occurs in between them. Experimental progress on more than one dot has naturally been slower, but theoretical work has shown that optical manipulation of strongly interacting QD molecules can lead to spin entanglement (8) with relatively simple pulses (85).

A potential drawback of using trion states to manipulate single spins is that the charge configuration of the system can change significantly during a control pulse. This can lead to a strong phonon coupling (86) and to decoherence. However, by using chirped pulses or slow amplitude modulation, this decoherence channel can be strongly suppressed (9, 87–89).

4.5. Single-Shot Measurement

The measurements so far discussed have relied on weak dispersive effects in the case of QDs, or small changes to the fluorescence over a limited time window in the case of NV^- centers. A full measurement of a single spin is a rather slow process, and each of the experiments we have described prepares and measures the spin many times over to build up enough statistics to prove the correlation between the initialized state and the measured state. For most quantum computing applications, this will not be enough. Rather, high-fidelity single-shot determination of an unknown spin is required, and for this a much stronger spin-photon coupling must be engineered and exploited.

The first step toward this ideal in QDs was a demonstration that spins can be measured at resonance. Under this condition, the effect of a QD on a photon is greater than it can be in a detuned, dispersive setup. If a two-level system is driven resonantly, and the coupling between photon and exciton is stronger than the exciton decoherence rate, then the eigenstates of the system become polaritons (states with both photon and exciton character). Moreover, the emission spectrum changes from a single Lorentzian to a Mollow triplet (90), with two side bands split from the central peak by the QD-photon coupling. [Both upper and lower levels spilt into doublets; the observed spectral triplet occurs because two of the four transitions are degenerate. If the transition to a third level from one of the two doublets is probed, two distinct lines are observed as expected (91, 92).] It is a significant experimental challenge to observe the Mollow triplet, because the sidebands can be obscured by Rayleigh scattering of the incident light beam. However, Flagg et al. (93) overcame this problem by sandwiching the QD between two distributed Bragg reflector mirrors. Laser light is coupled into the layer between the mirrors using an optical fiber, and confined there by total internal reflection. The emission is then observed in a perpendicular direction to reduce any interference from the excitation beam. Shortly after this experiment, another group observed a quintuplet (94), in which the sidebands are spin-split in an applied magnetic field. However, this kind of measurement is not immune from spin-flip Raman processes, which still occur at a faster rate than the readout can be performed. In a recent demonstration of single-shot optical measurement (95), two QDs

are used so that the initial spin and readout exciton are spatially located in different dots. The readout process then proceeds through a trion consisting of two electrons with parallel spins and a heavy hole, and from this state electron spin-flips through Raman processes are not possible.

In NV^- centers, the emphasis has been on increasing the efficiency of optical coupling, for example, using microcavities based on silicon microspheres (96) or on-chip designs using GaP (97). Other approaches include the use of nanostructured diamond itself for optical confinement [e.g., diamond nanowires (98)] or using photonic crystal cavities that can be deterministically positioned to maximize coupling with the NV^- center (99).

4.6. Single-Photon Coupling and Entanglement

A more ambitious goal is to achieve single-shot measurement by detecting a single photon. If this could be achieved, it would permit the creation of spin entanglement between two matter-based electron spins placed at distant locations (100). We describe how this could be done using QDs (see **Figure 5**); however, similar schemes have been proposed for NV^- centers (101). Imagine two QDs in different places with the kind of spin selectivity discussed above, and that polarized light is used to drive just one of the two transitions in both QDs. Each QD is first initialized in the state $(|\uparrow\rangle + |\downarrow\rangle)/\sqrt{2}$ so that following optical excitation we have the state

$$|\Psi\rangle = \frac{1}{2}\left(|\downarrow\downarrow\rangle + |\downarrow T_h^{\uparrow}\rangle + |T_h^{\uparrow}\downarrow\rangle + |T_h^{\uparrow}T_h^{\uparrow}\rangle\right). \quad 2.$$

This will eventually decay back to the ground state, with the emission of either no photons (corresponding to the first term on the right-hand side of Equation 2), one photon (second and third terms), or two photons (last term). The QDs are placed inside cavities such that the emission is almost always in the directions shown. If the detectors can discriminate between different photon numbers, but they register just one photon between them, then the system is projected into the state corresponding to the decay products of the second and third terms. Importantly, we cannot tell which one, because each passes through a 50:50 beamsplitter before being detected, and if the QDs are identical this erases any information about which path the photon takes before the beamsplitter. We are therefore projected into an entangled state of the form $(|\uparrow\downarrow\rangle + \exp(i\phi)|\downarrow\uparrow\rangle)/\sqrt{2}$, with the phase factor determined by which detector fires.

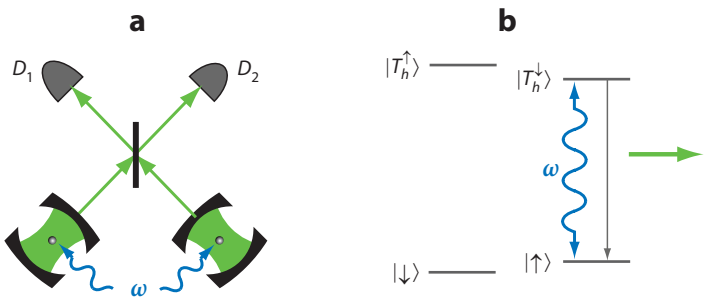

Figure 5

(*a*) Schematic diagram showing the experimental setup needed for the creation of entanglement by measurement. Two quantum dots (QDs) are embedded in cavities to enhance emission into the modes shown. Two detectors D_1 and D_2 are placed downstream of a beamsplitter; detection of one photon heralds an entangled spin state. (*b*) Required level structure of the QD. (Figure adapted and reprinted with permission from Reference 2.)

Several theoretical ideas for entanglement creation along these lines have been put forward over the past few years (101–105), and aspects of these have been demonstrated in ion traps and atomic ensembles (106, 107). The most important feature of this kind of entanglement creation is that is it heralded: We know when our operation works and when it fails simply by counting detection photons.

By performing successful entangling measurements on adjacent pairs of spins, a large entangled resource can be built up. NV^- centers possess a local, coupled nuclear spin that is immune to the optical excitation performed while attempting to create electron spin entanglement, and this allows a broker-client approach to efficiently build up larger entangled states (108). Any quantum algorithm can be performed using such a resource simply by making single-qubit measurements (2, 109).

Controlled entanglement of a single spin and a single photon would represent the ultimate interface of the two degrees of freedom (110). Such a static-to-flying qubit interconversion would allow for secure quantum communication (111) and the construction of truly quantum networks (112). Certain key aspects such as strong dot-cavity coupling (113–115) have been experimentally demonstrated, and recently (non-deterministic) entanglement between a single spin and a photon was detected in the NV^- system (116).

5. ELECTRON SPIN—CHARGE COUPLING

5.1. Electrically Detected Magnetic Resonance

The relationship between electrical conductivity and the spin states of conduction and localized electrons within a material has been exploited for some time in the technique of electrically detected magnetic resonance (117–119). Although the effect is often very weak—only a small fraction of a percent change in conductivity—it offers an opportunity to detect and measure small numbers of electron spins (< 100) by measuring the conductivity of nanostructured devices (120).

Three primary mechanisms for electrically detected magnetic resonance have been used to measure electron spins in semiconductors: spin-dependent scattering (121, 122), spin-dependent recombination (120), and spin-dependent tunneling (123). Spin-dependent scattering is observed in metal-oxide-semiconductor field-effect transistor structures, in which the scattering cross section of a 2DEG electron and a bound donor electron depends on their relative spin orientation (i.e., singlet versus triplet) (121).

Spin-dependent recombination involves first optically generating charge carriers in the material, which then recombine via charge traps. Commonly, this technique involves two species of charge trap, such as a dangling bond P_{b0} center in silicon coupled, for example, to a P-donor (124). If the two trapped charges are in the singlet (versus the triplet) state, the P-donor will transfer its electron to the P_{b0} center, and subsequently capture an electron from the conduction band. Recombination then takes place between the P_{b0}^- state and a hole, such that the overall process reduces the carrier concentration and thus the conductivity of the device. An alternative is to use just one charge trap, such as the P-donor itself, which ionizes to the D^- state when trapping a conduction electron (125). Trapping is only possible when the conduction spin and trap spin are in a singlet state, which leads to a measurable change in the recombination rate if both spins are highly polarized, requiring high magnetic fields and low temperatures (e.g., > 3 T and < 4 K). This has the advantage of being able to measure donor spins that are not necessarily coupled to interface defects that lead to shorter relaxation times (126).

Various approaches have been proposed and explored to extend these ideas to the single-spin level—in most cases, this involves scaling the devices used down to a sufficiently small scale so

Quantum point contact (QPC): narrow constriction between two conducting regions whose conductance is extremely sensitive to nearby charge

that the behavior of a single donor has a nonnegligible impact on the conductivity of the device (127, 128). It is also possible to use the donor nuclear spin as an ancilla for repetitive measurement to enhance the sensitivity (129).

Although these methods could ultimately be used to measure a single-spin state, they do so using a large number of electronic charges—analogous to the way spins can be measured through an optical fluorescence or polarization change detected using a large number of photons. We now examine how the state of a single charge can be coupled to an electron spin, offering a powerful electrical method for initializing, measuring, and manipulating single spins.

5.2. Single-Charge Experiments

As discussed in Section 2.1, the charge state of lithographically defined QDs can be controlled by applying voltages to gate electrodes, and the isolation of just a single electron in a QD was achieved many years ago (see Reference 130 for a detailed review of achievements in the 1990s in QD electron control). In the past decade, experiments have shown the conversion of information carried by single spins into measurable single-charge effects, so-called spin-to-charge conversion. Several excellent reviews of this topic already exist (5, 131); thus, here we touch on a few key early results, and then focus on some more recent achievements.

An early measurement of single-spin dynamics that used a form of spin-to-charge conversion was achieved by Fujisawa et al. in 2002 (132). They demonstrated that a single QD could be filled with one or two electrons by applying a particular voltage to the QD gate electrode, states which they termed artificial hydrogen and helium atoms. In the two-electron case, the authors demonstrated that the number of charges escaping from the QD can be made proportional to triplet population, and in this way triplet-to-singlet relaxation times were probed.

Single-shot readout of a single spin was achieved two years later (133), using a single gate-defined QD in a magnetic field that is tunnel coupled to a reservoir at one side, and has a quantum point contact (QPC) at the other side. A QPC is a one-dimensional channel for charge transport, whose conductance rises in discrete steps as a function of local voltage (134, 135). By tuning the QPC to the edge of one of these steps, a conductance measurement can act as a sensitive charge detector. The QD is first loaded with a single electron by raising the potential of the plunger gate, which transfers a random spin from the reservoir. After a controlled waiting time, the voltage is lowered to a level such that the two Zeeman split spin levels straddle the Fermi surface of the reservoir. It is therefore only possible for the spin-up state to tunnel out, an event that can be picked up by the QPC. Such spin-dependent tunneling lies at the heart of almost all spin-to-charge conversion measurements in these kinds of systems. By repeating the procedure many times, and for different waiting times, it is possible to measure the electron spin relaxation time (T_1).

Coherence times (T_2) of electron spins can be probed using a similar single-shot readout technique: Petta et al. (136) did this using a double QD loaded with two electrons. Depending on the relative potentials of the two dots, the electrons can be either on the same dot [labeled (1, 1)] or on different dots [(2, 0)]. A nearby QPC is sensitive to charge on one of the two dots and so can distinguish these two situations. Importantly, for (2, 0) the electrons must be in the singlet state, due to Pauli's exclusion principle. This provides means of initializing and reading out (1, 1) states: A triplet (1, 1) will not tunnel to (2, 0) when the dot detuning is changed to make (2, 0) the ground state, but a singlet will. In this way, the dynamics of a qubit defined by the singlet and the triplet state with zero spin projection can probed. Because these two states differ only by a phase, this leads to a measurement of the dephasing T_2 time, which is found to be primarily dependent on the interactions with the nuclear spins on the Ga and As atoms.

Though it is possible to remove the effects of static nuclear spins through rephasing techniques, nuclear spin fluctuations limit T_2 to the microsecond regime.

SET: single-electron transistor

More recent achievements have focused on the manipulation of electron spins using ESR, permitting the observation of Rabi oscillations. For example, in Reference 137, an oscillating magnetic field is applied to a two-QD system by applying a radio-frequency signal to an on-chip coplanar stripline. The resulting Rabi oscillations can be picked up by measuring the current through the device following the radio-frequency pulse; Pauli's exclusion principle means that the current is maximized for antiparallel spins. In an alternative approach, a magnetic field gradient was applied across a two-QD device using a ferromagnetic strip so that field strength depended on the equilibrium position of the electron charge (138). The application of an oscillating electric field induces an oscillation of the electron charge—the electron spin then feels a periodic modulation of the magnetic field. If the modulation is at a frequency corresponding to the spin resonance condition, then Rabi oscillations occur.

The past two or three years have seen a considerable improvement in our understanding and control of the primary electron spin decoherence mechanism: interactions with the GaAs nuclear spin bath. For example, the nuclear spin bath can be polarized by transferring angular momentum from the electron spins (139), resulting in a narrower field distribution. The nuclear spin field can also adjust itself so that the condition for ESR is satisfied for a range of applied fields (140); this may also result in a reduction in electron spin dephasing by narrowing the nuclear field distribution. Remarkably, fast single-shot readout of an electron spin has permitted the static nuclear field to be measured and tracked through the real-time impact it has on the singlet-triplet qubit discussed above (141).

Removing nuclear spins altogether is also possible, for example, by using QDs in silicon- or carbon-based devices such as those fabricated using graphene or carbon nanotubes (142). Demonstration of a single spin-to-charge conversion has now been observed in silicon using a single-electron transistor (SET) (20), as described in **Figure 6**, and the demonstration of the coherent exchange of electrons between two donors (143) may provide a route to generating spin entanglement.

6. ELECTRON SPIN AND SUPERCONDUCTING QUBITS

Qubits based on charge-, flux-, or phase-states in superconducting circuits can be readily fabricated using standard lithographic techniques and can afford one an impressive degree of quantum control (144). Multiple superconducting qubits can be coupled together through their mutual interaction with on-chip microwave stripline resonators (145). These methods have been used to demonstrate the violation of Bell's inequalities (146) and to create three-qubit entangled states (147, 148).

The weakness of superconducting qubits remains their short decoherence times, typically limited to a few microseconds, depending on the species of qubit (144): For example, coherence times in the three-qubit device of Reference 148 were limited to less than a microsecond. Electron spins, in contrast, can have coherence times up to 10 s in the solid state, and typically operate at similar microwave frequencies as superconducting qubits. The possibility of transferring quantum information between superconducting qubits and electron spins is therefore attractive.

Although it is possible to convert a superconducting qubit state into a cavity microwave photon (3), achieving direct strong coupling between such a photon and a single-electron spin appears beyond the capabilities of current technology. [A superconducting cavity could be used for single-spin ESR (see sidebar on Single-Spin Electron Spin Resonance); however,

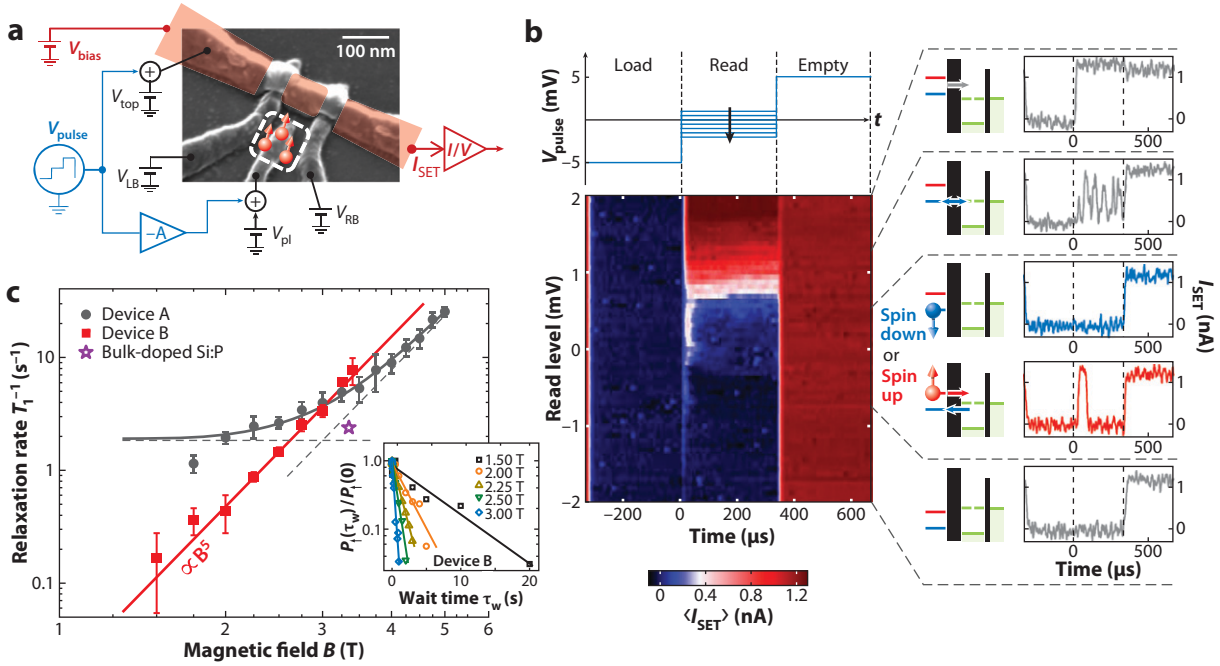

Figure 6

Single-shot single spin-to-charge conversion in silicon using a metal-oxide-semiconductor (MOS) single-electron transistor (SET). (*a*) P-donors are implanted within the vicinity of the SET island, underneath a plunger gate V_{pl}, which controls their potential with respect to the SET. Statistically, one expects ~3 donors to be sufficiently tunnel coupled to the SET. (*b*) An electron can be loaded onto the donor by making the chemical potential μ_{donor} much lower than that of the SET island μ_{SET}. Placing μ_{SET} in between the spin-up and spin-down levels of the donor enables spin-dependent tunneling of the donor electron back onto the SET island. (*c*) The electron spin relaxation time T_1 is measured by loading an electron (with a random spin state) onto the donor, followed by a measurement of the spin some variable time later. The B^5 magnetic field dependence, and absolute values of T_1 measured, is consistent with a P-donor electron spin (S. Simmons, R.M. Brown, H. Riemann, N.V. Abrosimov, P. Becker, et al., unpublished observation). (Reprinted with permission from Reference 20, with permission from Macmillan Publishers Ltd.)

this application places fewer demands on the coupling and cavity/spin linewidths than a quantum memory.] Instead, the spin-cavity coupling (which scales as $\sqrt{N}$ for N spins) can be enhanced by placing a larger ensemble of spins within the mode volume of the cavity, thus ensuring that a microwave photon in the cavity is absorbed into a collective excited state of the ensemble. The apparent wastefulness of resources (one photon stored in many spins) can be overcome by using holographic techniques to store multiple excitations in orthogonal states within the ensemble (149), as has been explored extensively in optical quantum memories (150).

A key step in demonstrating a solid-state microwave photon quantum memory based on electron spins is to demonstrate strong coupling between an electron spin ensemble and single microwave photons in a superconducting resonator. Typically, electron spins are placed in a magnetic field to achieve transition frequencies in the GHz regime; however, such fields can adversely affect the performance of superconducting resonators. One solution is to apply the magnetic field strictly parallel to the plane of thin film superconductors—this has been used to observe coupling to *a*) the organic radical DPPH deposited over the surface of the resonator; *b*) paramagnetic Cr^{3+} centers within the ruby substrate on which the resonator is fabricated;

and *c*) substitutional nitrogen defects within a sample of diamond glued onto the top of the niobium resonator (see **Figure 7***a*) (25). Another solution is to seek out electron spins that possess microwave transition frequencies in the absence of an applied magnetic field—indeed this would appear the most attractive, because the superconducting qubits themselves (which are generally made of aluminum) are unlikely to survive even modest magnetic fields. Thanks to their zero-field splitting of ∼3 GHz, NV^- centers in diamond have been used to observe strong coupling to a frequency-tuneable superconducting resonator in the absence of an appreciable magnetic field ($B < 3$ mT) (26) (see **Figure 7***b*). The ability to rapidly tune the resonator into resonance with the spin ensemble should enable the observation of coherent oscillations between the two, and ultimately, the storage of a single microwave photon in the spin ensemble.

An alternative approach is to couple an electron spin, or spins, directly to the superconducting qubit, as proposed by Marcos et al., using the magnetic field from a flux qubit (151), or similarly, to boost the coupling of a superconducting resonator to a single spin through the use of a persistent current loop (152). Having stored the superconducting qubit state within a collective state of electron spins (through any of the above approaches), it is then

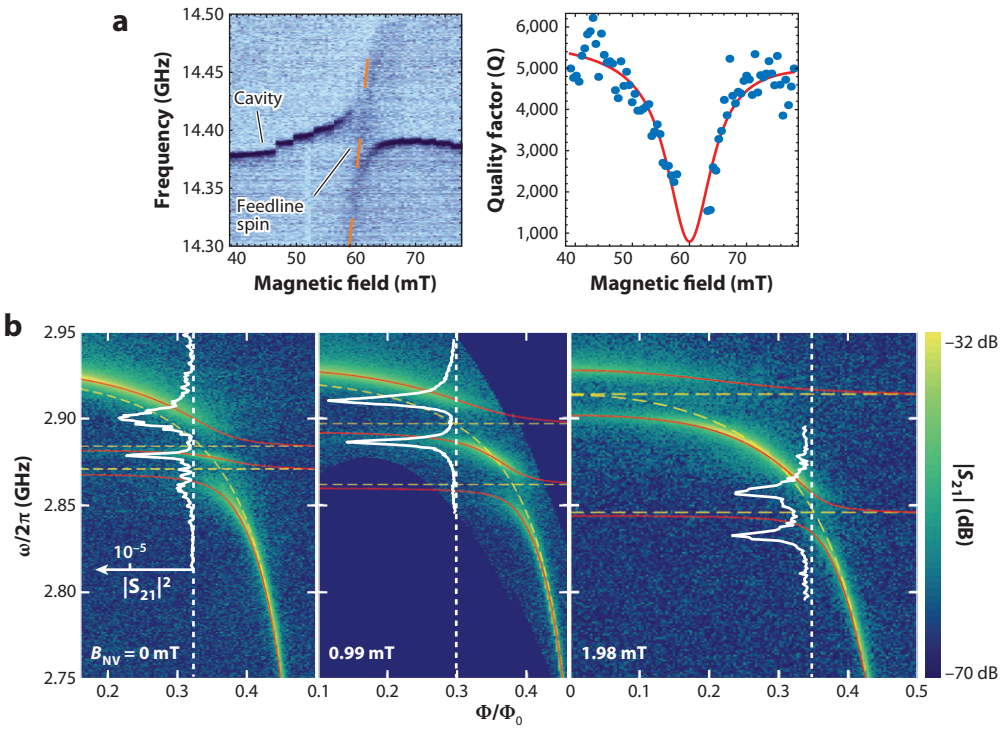

Figure 7

(*a*) The transmission spectrum of a superconducting stripline microwave resonator, fabricated on a ruby substrate, as a function of magnetic field. A coupling strength of 38 MHz is observed between the resonator and $\sim 10^{12}$ Cr^{3+} spins ($S = 3/2$) located in the substrate, within the mode volume of the resonator. (*b*) The transmission $|S_{21}|$ of a resonator with a diamond on top shows two anticrossings arising from the two $\Delta m_s = 1$ transitions of the NV^- center, whose frequencies shift in opposite directions under a weak applied magnetic field B_{NV}. The resonator itself incorporates a superconducting quantum interference device (SQUID) array, allowing frequency tuning through a locally applied magnetic flux Φ. Red (*yellow*) lines are fits to the eigenfrequencies of the coupled (uncoupled) resonator/spin-ensemble system. Panels *a* and *b* reprinted with permission from References 25 and 26, respectively, Copyright (2010) by the American Physical Society.

possible in principle to transfer their state into a collective state of nuclear spins (153), using the coherence transfer methods described in Section 3, thus benefitting from the longer nuclear coherence times.

7. SUMMARY AND OUTLOOK

In this review, we have attempted to systematically look at the coupling of electron spin to other degrees of freedom capable of hosting quantum information: nuclear spin, charge, optical photons, and superconducting qubits. We have not been able to cover all possibilities. For example, we have not mentioned electron spins coupled to mechanical states, which are explored in a recent proposal (160).

In many cases, substantial benefit arises from bringing together more than one of the hybridizing schemes discussed in this review. For example, in NV^- centers, one can combine three degrees of freedom: the optical electronic transition, the electron spin, and the nuclear spin of a nearby ^{13}C. Alternatively, a hybrid electrical and optical method for measuring single-electron or nuclear spin states of P-donors in silicon has been demonstrated that exploits the ability to selectively optically excite a bound exciton state of the P-donor and a nearby QPC (161).

Nevertheless, it is clear that electron spins play an essential role in a wide range of proposals for hybridizing quantum information in the solid state. This can be attributed to their balance of portability, long-lived coherent behavior, and versatility in coupling to many varied degrees of freedom.

SUMMARY POINTS

1. A versatile qubit can be represented in the electron spin of quantum dot (QDs), impurities in solids, organic molecules, and free electrons in the solid state.
2. A coupled electron spin can provide many advantages to a nuclear spin qubit, including high fidelity initialization, manipulation on the nanosecond timescale, and more sensitive measurement.
3. The state of an electron spin can be coherently stored in a coupled nuclear spin, offering coherence times exceeding seconds (**Figure 3**).
4. The interaction of an electron spin with many optical photons can be used for single-spin measurement (**Figure 4**), and manipulation on the picosecond timescale, whereas coupling to a single photon could be used to generate entanglement between two macroscopically separated electron spins (**Figure 5**).
5. The electron spin of lithographically defined QDs can be measured through spin-dependent tunneling between and off dots, and the use of a local quantum point contact (QPC).
6. A similar technique can been applied to the electron spin of a donor in silicon, the important difference being that the electron tunnels off the donor directly onto a single-electron transistor (SET) island, offering high-fidelity single-shot measurement (**Figure 6**).
7. Electron spin could be used to store the state of a superconducting qubit. An important step toward achieving this has been demonstrated in the observation of strong coupling between an electron spin ensemble and a superconducting microwave stripline resonator (**Figure 7**).

DISCLOSURE STATEMENT

The authors are not aware of any affiliations, memberships, funding, or financial holdings that might be perceived as affecting the objectivity of this review.

LITERATURE CITED

1. Nielsen MA, Chuang IL. 2000. *Quantum Computation and Quantum Information*. Cambridge, UK: Cambridge Univ. Press
2. Kok P, Lovett BW. 2010. *Introduction to Optical Quantum Information Processing*. Cambridge, UK: Cambridge Univ. Press
3. Wallraff A, Schuster DI, Blais A, Frunzio L, Huang RS, et al. 2004. *Nature* 431:162
4. Harrison P. 2000. *Quantum Wells, Wires and Dots*. Chichester: Wiley
5. Hanson R, Awschalom DD. 2008. *Nature* 453:1043–49
6. Ramsay AJ, Boyle SJ, Kolodka RS, Oliveira JBB, Skiba-Szymanska J, et al. 2008. *Phys. Rev. Lett.* 100:197401
7. Gerardot BD, Brunner D, Dalgarno PA, Ohberg P, Seidl S, et al. 2008. *Nature* 451:441–44
8. Calarco T, Datta A, Fedichev P, Pazy E, Zoller P. 2003. *Phys. Rev. A* 68:012310
9. Gauger EM, Benjamin SC, Nazir A, Lovett BW. 2008. *Phys. Rev. B* 77:115322
10. Mikkelsen MH, Berezovsky J, Stoltz NG, Coldren LA, Awschalom DD. 2007. *Nat. Phys.* 3:770–73
11. Xu XD, Wu YW, Sun B, Huang Q, Cheng J, et al. 2007. *Phys. Rev. Lett.* 99:097401
12. Basu PK. 1997. *Theory of Optical Processes in Semiconductors: Bulk and Microstructures*. Oxford: Oxford Univ. Press
13. Kane BE. 1998. *Nature* 393:133–37
14. Skinner A, Davenport M, Kane B. 2003. *Phys. Rev. Lett.* 90:87901
15. Morton JJL. 2010. A silicon-based cluster state quantum computer. arXiv:0905.4008
16. Ruess F, Oberbeck L, Simmons M, Goh K, Hamilton A, et al. 2004. *Nano Lett.* 4:1969–73
17. Calderón MJ, Koiller B, Hu X, Das Sarma S. 2006. *Phys. Rev. Lett.* 96:096802
18. Lansbergen GP, Rahman R, Wellard CJ, Woo I, Caro J, et al. 2008. *Nat. Phys.* 4:656–61
19. Bradbury FR, Tyryshkin AM, Sabouret G, Bokor J, Schenkel T, Lyon SA. 2006. *Phys. Rev. Lett.* 97:176404
20. **Morello A, Pla JJ, Zwanenburg FA, Chan KW, Huebl H, et al. 2010. *Nature* 467:687–91**
21. **Morton JJL, Tyryshkin AM, Brown RM, Shankar S, Lovett BW, et al. 2008. *Nature* 455:1085–88**
22. Stoneham A, Fisher A, Greenland P. 2003. *J. Phys.-Condens. Matter* 15:L447–51
23. George RE, Witzel W, Riemann H, Abrosimov N, Notzel N, et al. 2010. *Phys. Rev. Lett.* 105:067601
24. Morley GW, Warner M, Stoneham AM, Greenland PT, van Tol J, et al. 2010. *Nat. Mater.* 9:725–29
25. **Schuster DI, Sears AP, Ginossar E, DiCarlo L, Frunzio L, et al. 2010. *Phys. Rev. Lett.* 105:140501**
26. **Kubo Y, Ong FR, Bertet P, Vion D, Jacques V, et al. 2010. *Phys. Rev. Lett.* 105:140502**
27. Jelezko F, Gaebel T, Popa I, Domhan M, Gruber A, Wrachtrup J. 2004. *Phys. Rev. Lett.* 93:130501
28. Jelezko F, Gaebel T, Popa I, Gruber A, Wrachtrup J. 2004. *Phys. Rev. Lett.* 92:076401
29. Balasubramanian G, Neumann P, Twitchen D, Markham M, Kolesov R, et al. 2009. *Nat. Mater.* 8:383–87
30. **Neumann P, Kolesov R, Naydenov B, Beck J, Rempp F, et al. 2010. *Nat. Phys.* 6:249–53**
31. Sanaka K, Pawlis A, Ladd TD, Lischka K, Yamamoto Y. 2009. *Phys. Rev. Lett.* 103:053601
32. Guillot-Noël O, Goldner P, Le Du Y, Baldit E, Monnier P, Bencheikh K. 2008. *J. Alloys Compd.* 451:62–64
33. Jeschke G, Polyhach Y. 2007. *Phys. Chem. Chem. Phys.* 9:1895–1910
34. Lindgren M, Eaton GR, Eaton SS, Jonsson BH, Hammarström P, et al. 1997. *J. Chem. Soc. Perkin Trans.* 2:2549–54
35. Brown RM, Ito Y, Warner J, Ardavan A, Shinohara H, et al. 2010. *Phys. Rev. B* 82:033410
36. Morton JJL, Tyryshkin AM, Ardavan A, Porfyrakis K, Lyon SA, Briggs GAD. 2006. *J. Chem. Phys.* 124:014508

20. Demonstrates a single-shot single-spin measurement in silicon of what is most likely a P-donor.

21. Demonstrates storage and retrieval of a coherent electron spin state in a P-donor nuclear spin, giving a quantum memory lifetime exceeding seconds.

25, 26. Offer parallel demonstrations of coupling of spin ensembles to superconducting microwave stripline resonators at milliKelvin temperatures.

30. Using optical spin measurement, observes coupling between a single pair of NV^- centers in diamond, separated by ~100 Å.

37. Morton JJL, Tyryshkin AM, Ardavan A, Porfyrakis K, Lyon SA, Briggs GAD. 2007. *Phys. Rev. B* 76:085418
38. McConnell HM, Heller C, Cole T, Fessenden RW. 1960. *J. Am. Chem. Soc.* 82:766–75
39. Mehring M, Mende J, Scherer W. 2003. *Phys. Rev. Lett.* 90:153001
40. Mitrikas G, Sanakis Y, Papavassiliou G. 2010. *Phys. Rev. A* 81:020305
41. Leuenberger M, Loss D. 2001. *Nature* 410:789–93
42. Ardavan A, Rival O, Morton JJL, Blundell SJ, Tyryshkin AM, et al. 2007. *Phys. Rev. Lett.* 98:057201
43. Mitrikas G, Sanakis Y, Raptopoulou CP, Kordas G, Papavassiliou G. 2008. *Phys. Chem. Chem. Phys.* 10:743–48
44. Barnes CHW, Shilton JM, Robinson AM. 2000. *Phys. Rev. B* 62:8410–19
45. Sabouret G, Bradbury FR, Shankar S, Bert JA, Lyon SA. 2008. *Appl. Phys. Lett.* 92:082104
46. Lyon SA. 2006. *Phys. Rev. A* 74:052338
47. Cory DG, Fahmy AF, Havel TF. 1997. *Proc. Natl. Acad. Sci. USA* 94:1634–39
48. Gershenfeld NA, Chuang IL. 1997. *Science* 275:350–56
49. Vandersypen LMK, Steffen M, Breyta G, Yannoni C, Sherwood M, Chuang I. 2001. *Nature* 414:883–87
50. Braunstein SL, Caves CM, Jozsa R, Linden N, Popescu S, Schack R. 1999. *Phys. Rev. Lett.* 83:1054–57
51. Anwar M, Blazina D, Carteret H, Duckett S, Halstead T, et al. 2004. *Phys. Rev. Lett.* 93:040501
52. Maly T, Debelouchina GT, Bajaj VS, Hu KN, Joo CG, et al. 2008. *J. Chem. Phys.* 128:052211
53. Barnes AB, Paepe GD, van der Wel PCA, Hu KN, Joo CG, et al. 2008. *Appl. Magn. Reson.* 34:237–63
54. Davies ER. 1974. *Phys. Lett. A* 47:1–2
55. Tyryshkin A, Morton J, Ardavan A, Lyon S. 2006. *J. Chem. Phys.* 124:234508
56. Ryan CA, Moussa O, Baugh J, Laflamme R. 2008. *Phys. Rev. Lett.* 100:140501
57. Kagawa A, Negoro M, Takeda K, Kitagawa M. 2009. *Rev. Sci. Instrum.* 80:044705
58. Aharonov Y, Anandan J. 1987. *Phys. Rev. Lett.* 58:1593–96
59. Morton JJL, Tyryshkin AM, Ardavan A, Benjamin SC, Porfyrakis K, et al. 2006. *Nat. Phys.* 2:40–43
60. Tyryshkin AM, Benjamin JMS, Ardavan A, Briggs G, Ager JW, Lyon SA. 2006. *J. Phys.-Condens. Matter* 18:S783
61. Khaneja N. 2007. *Phys. Rev. A* 76:032326
62. Hodges J, Yang J, Ramanathan C, Cory D. 2008. *Phys. Rev. A* 78:010303
63. Khaneja N, Reiss T, Kehlet C, Schulte-Herbrüggen T, Glaser S. 2005. *J. Magn. Reson.* 172:296–305
64. Hahn EL, Maxwell DE. 1952. *Phys. Rev.* 88:1070–84
65. Dikanov SA, Tsvetkov YD. 1992. *Electron Spin Echo Envelope Modulation (ESEEM) Spectroscopy.* Boca Raton, FL: CRC Press
66. Schaffry M, Filidou V, Karlen SD, Gauger EM, Benjamin SC, et al. 2010. *Phys. Rev. Lett.* 104:200501
67. Mehring M, Scherer W, Weidinger A. 2004. *Phys. Rev. Lett.* 93:206603
68. Dutt MVG, Childress L, Jiang L, Togan E, Maze J, et al. 2007. *Science* 316:1312–16
69. Sekiguchi T, Steger M, Saeedi K, Thewalt MLW, Riemann H, et al. 2010. *Phys. Rev. Lett.* 104:137402
70. McCamey DR, van Tol J, Morley GW, Boehme C. 2009. *Phys. Rev. Lett.* 102:027601
71. Yang A, Steger M, Sekiguchi T, Thewalt MLW, Ladd TD, et al. 2009. *Phys. Rev. Lett.* 102:257401
72. Manson NB, Harrison JP, Sellars MJ. 2006. *Phys. Rev. B* 74:104303
73. Wrachtrup J, Jelezko F. 2006. *J. Phys.-Condens. Matter* 18:S807–24
74. Atatüre M, Dreiser J, Badolato A, Högele A, Karrai K, Imamoglu A. 2006. *Science* 312:551–53
75. Alen B, Bickel F, Karrai K, Warburton RJ, Petroff PM. 2003. *Appl. Phys. Lett.* 83:2235–37
76. Hogele A, Kroner M, Seidl S, Karrai K, Atatüre M, et al. 2005. *Appl. Phys. Lett.* 86:221905
77. Kroutvar M, Ducommun Y, Heiss D, Bichler M, Schuh D, et al. 2004. *Nature* 432:81–84
78. Jiang L, Hodges JS, Maze JR, Maurer P, Taylor JM, et al. 2009. *Science* 326:267–72
79. Steiner M, Neumann P, Beck J, Jelezko F, Wrachtrup J. 2010. *Phys. Rev. B* 81:035205
80. Jiang L, Dutt MVG, Togan E, Childress L, Cappellaro P, et al. 2008. *Phys. Rev. Lett.* 100:073001
81. Berezovsky J, Mikkelsen MH, Gywat O, Stoltz NG, Coldren LA, Awschalom DD. 2006. *Science* 314:1916–20

59. Shows manipulation of the nuclear spin through microwave operations on the electron spin, and the use of this in dynamic decoupling.

82. Atatüre M, Dreiser J, Badolato A, Imamoglu A. 2007. *Nat. Phys.* 3:101–6
83. Berezovsky J, Mikkelsen MH, Stoltz NG, Coldren LA, Awschalom DD. 2008. *Science* 320:349–52
84. Greilich A, Economou SE, Spatzek S, Yakovlev DR, Reuter D, et al. 2009. *Nat. Phys.* 5:262–66
85. Nazir A, Lovett BW, Barrett SD, Spiller TP, Briggs GAD. 2004. *Phys. Rev. Lett.* 93:150502
86. Ramsay AJ, Gopal A, Gauger EM, Nazir A, Lovett BW, et al. 2010. *Phys. Rev. Lett.* 104:017402
87. Lovett BW, Nazir A, Pazy E, Barrett SD, Spiller TP, Briggs GAD. 2005. *Phys. Rev. B* 72:115324
88. Gauger EM, Nazir A, Benjamin SC, Stace TM, Lovett BW. 2008. *N. J. Phys.* 10:073016
89. Roszak K, Grodecka A, Machnikowski P, Kuhn T. 2005. *Phys. Rev. B* 71:195333
90. Mollow BR. 1969. *Phys. Rev.* 188:1969–75
91. Xu X, Sun B, Berman PR, Steel DG, Bracker AS, et al. 2007. *Science* 317:929–32
92. Boyle SJ, Ramsay AJ, Fox AM, Skolnick MS, Heberle AP, Hopkinson M. 2009. *Phys. Rev. Lett.* 102:207401
93. Flagg EB, Muller A, Robertson JW, Founta S, Deppe DG, et al. 2009. *Nat. Phys.* 5:203–7
94. Vamivakas AN, Zhao Y, Lu CY, Atatüre M. 2009. *Nat. Phys.* 5:198–202
95. Vamivakas AN, Lu CY, Matthiesen C, Zhao Y, Fält S, et al. 2010. *Nature* 467:297–300
96. Larsson M, Dinyari K, Wang H. 2009. *Nano Lett.* 9:1447–50
97. Barclay P, Fu K, Santori C. 2009. *Appl. Phys. Lett.* 95:191115
98. Babinec TM, Hausmann BJM, Khan M, Zhang Y, Maze JR, et al. 2010. *Nat. Nanotechnol.* 5:195–99
99. Englund D, Shields B, Rivoire K, Hatami F, Vuckovic J, et al. 2010. *Nano Lett.* 10:3922–26
100. Benjamin SC, Lovett BW, Smith JM. 2009. *Lasers Photonics Rev.* 3:556–74
101. Barrett SD, Kok P. 2005. *Phys. Rev. A* 71:060310
102. Cabrillo C, Cirac JI, Garcia-Fernández P, Zoller P. 1999. *Phys. Rev. A* 59:1025–33
103. Bose S, Knight PL, Plenio MB, Vedral V. 1999. *Phys. Rev. Lett.* 83:5158–61
104. Lim YL, Beige A, Kwek LC. 2005. *Phys. Rev. Lett.* 95:030505
105. Kolli A, Lovett BW, Benjamin SC, Stace TM. 2006. *Phys. Rev. Lett.* 97:250504
106. Moehring DL, Maunz P, Olmschenk S, Younge KC, Matsukevich DN, et al. 2007. *Nature* 449:68–71
107. Laurat J, Choi KS, Deng H, Chou CW, Kimble HJ. 2007. *Phys. Rev. Lett.* 99:180504
108. Benjamin SC, Browne DE, Fitzsimons J, Morton JJL. 2006. *N. J. Phys.* 8:141
109. Raussendorf R, Briegel HJ. 2001. *Phys. Rev. Lett.* 86:5188–91
110. Yao W, Liu RB, Sham LJ. 2005. *Phys. Rev. Lett.* 95:030504
111. DiVincenzo DP. 2000. *Fortschr. Phys.* 48:771–83
112. Cirac JI, Ekert AK, Huelga SF, Macchiavello C. 1999. *Phys. Rev. A* 59:4249–54
113. Yoshie T, Scherer A, Hendrickson J, Khitrova G, Gibbs HM, et al. 2004. *Nature* 432:200–3
114. Reithmaier JP, Sek G, Löffler A, Hofmann C, Kuhn S, et al. 2004. *Nature* 432:197–200
115. Hennessy K, Badolato A, Winger M, Gerace D, Atatüre M, et al. 2007. *Nature* 445:896–99
116. Togan E, Chu Y, Trifonov AS, Jiang L, Maze J, et al. 2010. *Nature* 466:730–34
117. Schmidt J, Solomon I. 1966. *Compt. Rend.* 263:169
118. Lepine DJ. 1972. *Phys. Rev. B* 6:436–41
119. Brandt MS, Goennenwein STB, Graf T, Huebl H, Lauterbach S, Stutzmann M. 2004. *Phys. Status Solidi C* 1:2056–2093
120. McCamey DR, Huebl H, Brandt MS, Hutchison WD, McCallum JC, et al. 2006. *Appl. Phys. Lett.* 89:182115
121. Ghosh R, Silsbee R. 1992. *Phys. Rev. B* 46:12508–25
122. Lo CC, Bokor J, Schenkel T, Tyryshkin AM, Lyon SA. 2007. *Appl. Phys. Lett.* 91:242106
123. Ryan JT, Lenahan PM, Krishnan AT, Krishnan S. 2009. *Appl. Phys. Lett.* 95:103503
124. Stegner AR, Boehme C, Huebl H, Stutzmann M, Lips K, Brandt MS. 2006. *Nat. Phys.* 2:835–38
125. Morley GW, McCamey DR, Seipel HA, Brunel LC, van Tol J, Boehme C. 2008. *Phys. Rev. Lett.* 101:207602
126. Paik SY, Lee SY, Baker WJ, McCamey DR, Boehme C. 2010. *Phys. Rev. B* 81:075214
127. van Beveren LHW, Huebl H, McCamey DR, Duty T, Ferguson AJ, et al. 2008. *Appl. Phys. Lett.* 93:072102
128. Lo CC, Persaud A, Dhuey S, Olynick D, Borondics F, et al. 2009. *Semicond. Sci. Technol.* 24:105022

83. Demonstrates optical initialization, manipulation, and measurement of a single spin in a quantum dot.

94. Demonstrates spin-dependent resonant fluorescence in a quantum dot.

100. Reviews measurement-based quantum computing in solid-state systems.

129. Sarovar M, Young KC, Schenkel T, Whaley KB. 2008. *Phys. Rev. B* 78:245302
130. Kouwenhoven LP, Austing DG, Tarucha S. 2001. *Rep. Prog. Phys.* 64:701–36
131. Hanson R, Kouwenhoven LP, Petta JR, Tarucha S, Vandersypen LMK. 2007. *Rev. Mod. Phys.* 79:1217–65
132. Fujisawa T, Austing DG, Tokura Y, Hirayama Y, Tarucha S. 2002. *Nature* 419:278–81
133. Elzerman JM, Hanson R, van Bereven LHW, Witkamp B, Vandersypen LM, Kouwenhoven LP. 2004. *Nature* 430:431–35
134. Wharam DA, Thornton TJ, Newbury R, Pepper M, Ahmed H, et al. 1988. *J. Phys. C* 21:L209–14
135. van Wees BJ, van Houten H, Beenakker CWJ, Williamson JG, Kouwenhoven LP, et al. 1988. *Phys. Rev. Lett.* 60:848–50
136. Petta JR, Johnson AC, Taylor JM, Laird EA, Yacoby A, et al. 2005. *Science* 309:2180–84
137. Koppens FHL, Buizert C, Tielrooij KJ, Vink IT, Nowack KC, et al. 2006. *Nature* 442:766–71
138. Pioro-Ladriére M, Obata T, Tokura Y, Shin YS, Kubo T, et al. 2008. *Nat. Phys.* 4:776–79
139. Reilly DJ, Taylor JM, Petta JR, Marcus CM, Hanson MP, Gossard AC. 2008. *Science* 321:817–21
140. Vink IT, Nowack KC, Koppens FHL, Danon J, Nazarov YV, Vandersypen LMK. 2009. *Nat. Phys.* 5:764
141. Barthel C, Reilly DJ, Marcus CM, Hanson MP, Gossard AC. 2009. *Phys. Rev. Lett.* 103:160503
142. Biercuk MJ, Garaj S, Mason N, Chow JM, Marcus CM. 2005. *Nano Lett.* 5:1267–71
143. Verduijn J, Tettamanzi GC, Lansbergen GP, Collaert N, Biesemans S, Rogge S. 2010. *Appl. Phys. Lett.* 96:072110
144. Clarke J, Wilhelm FK. 2008. *Nature* 453:1031–42
145. Niskanen AO, Harrabi K, Yoshihara F, Nakamura Y, Lloyd S, Tsai JS. 2007. *Science* 316:723–26
146. Ansmann M, Wang H, Bialczak RC, Hofheinz M, Lucero E, et al. 2009. *Nature* 461:504–6
147. Neeley M, Bialczak RC, Lenander M, Lucero E, Mariantoni M, et al. 2010. *Nature* 467:570–73
148. DiCarlo L, Reed MD, Sun L, Johnson BR, Chow JM, et al. 2010. *Nature* 467:574–78
149. Wesenberg JH, Ardavan A, Briggs GAD, Morton JJL, Schoelkopf RJ, et al. 2009. *Phys. Rev. Lett.* 103:070502
150. Reim KF, Nunn J, Lorenz VO, Sussman BJ, Lee KC, et al. 2010. *Nat. Photonics* 4:218–21
151. Marcos D, Wubs M, Taylor JM, Aguado R, Lukin MD, Sørensen AS. 2010. *Phys. Rev. Lett.* 105:210501
152. Twamley J, Barrett SD. 2010. *Phys. Rev. B* 81:241202
153. Wu H, George RE, Ardavan A, Wesenberg JH, Mølmer K, et al. 2010. *Phys. Rev. Lett.* 105:140503
154. Maze JR, Stanwix PL, Hodges JS, Hong S, Taylor JM, et al. 2008. *Nature* 455:644–47
155. Balasubramanian G, Chan IY, Kolesov R, Al-Hmoud M, Tisler J, et al. 2008. *Nature* 455:648–51
156. Chorley SJ, Giavaras G, Wabnig J, Jones GAC, Smith CG, et al. 2010. Single spin detection with a carbon nanotube double quantum dot. arXiv:1004.4377v1
157. Rodriguez-Manzo JA, Banhart F. 2009. *Nano Lett.* 9:2285–89
158. Wabnig J, Lovett BW. 2009. *N. J. Phys.* 11:043031
159. Giavaras G, Wabnig J, Lovett BW, Jefferson JH, Briggs GAD. 2010. *Phys. Rev. B* 82:085410
160. Rabl P, Kolkowitz S, Koppens F, Harris J, Zoller P, Lukin M. 2010. *Nat. Phys.* 6:602–8
161. Sleiter D, Kim NY, Nozawa K, Ladd TD, Thewalt MLW, Yamamoto Y. 2010. *N. J. Phys.* 12:093028
162. Koiller B, Hu X, Capaz RB, Martins AS, Das Sarma S. 2005. *An. Acad. Bras. Cienc.* 77: 201–22

131. Reviews the principles behind spin-to-charge conversion in quantum dots.